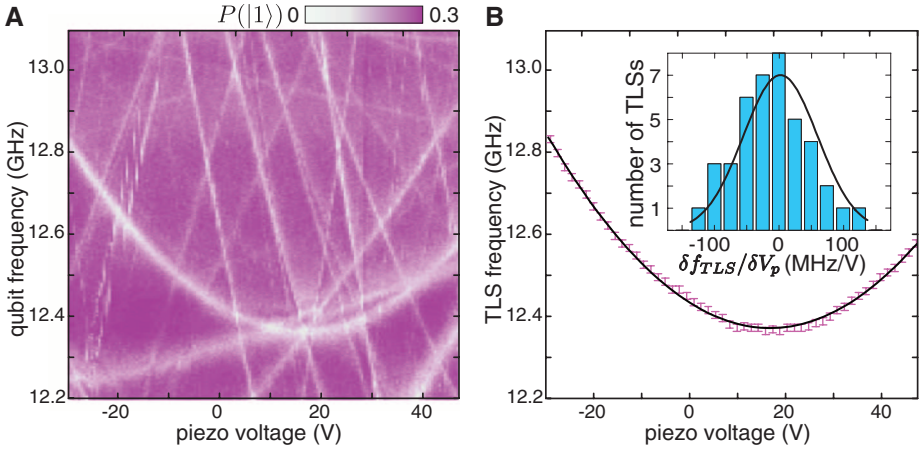

Fig. 4. Tuning two-level systems by strain. (**A**) At each value of V_p, a spectroscopic line like that shown in Fig. 3B is recorded. The resonance frequencies of the TLSs ($f_{TLS} = E/h$ as a function of V_p) appear lighter in color. The frequency dependence of the TLS showing a broad nonmonotonic behavior is extracted and fitted to a hyperbola given by Eq. 2 in (**B**). The error bars correspond to the width of the resonance dips. The inset in (B) shows the distribution of the linear frequency changes of the TLSs with respect to the voltage change; the solid line shows a Gaussian distribution for comparison.

for all TLSs, it can only be observed for TLSs that have their symmetry-point energy splitting in the accessible range limited by the tunability of the phase qubit. The other TLSs have tunnel energies Δ_0 much smaller than what is experimentally accessible; hence, only the nearly linear tails of their energy hyperbolas are observed. Data taken in the same way on another sample (fig. S4) (*23*) reveal five TLS traces obeying a hyperbolic frequency dependence on strain, showing that this is a common property of TLSs.

Another interesting trace in Fig. 4A, appearing between –30 and –10 V, indicates a TLS whose resonance frequency shifts at the rate of ~50 MHz/V and jumps randomly, within hours, between two traces ~100 MHz apart. Most likely, the local potential landscape of the coherent TLS under observation changes abruptly due to a nearby incoherent TLS fluctuating slowly and randomly between its localized states.

The basic idea of the above experiment has some similarity to earlier experiments (*30*, *31*) in which static strain was used to change the dwell times of individual incoherent TLSs (two-level fluctuators) in disordered metallic nanostructures. The experiments here are performed with individual coherent TLSs that have tunneling energies Δ_0 on the order of k_BT (where k_B is the Boltzmann constant and T is temperature) and asymmetry energies Δ tunable by strain from values on the order of k_BT to zero. The TLS energies E are measured directly, and their strain dependence given by Eq. 2 is confirmed.

All results presented above are explained readily by the tunneling model and, therefore, provide firm evidence of the hypothesis that atomic TLSs are the cause of avoided level crossings in the spectra of JJ qubits. Mechanical strain offers a handle to control the properties of coherent TLSs, which is crucial for gaining knowledge about their physical nature. Our method can also be used to tune TLS frequencies away from the qubit resonance and, thus, to optimize the coherence of a qubit circuit at its operation point. Moreover, the knowledge of how individual coherent TLSs are modified by strain opens an opportunity to manipulate TLSs via ultrasonic excitation.

References and Notes

1. R. C. Zeller, R. O. Pohl, *Phys. Rev. B* **4**, 2029 (1971).
2. W. A. Phillips, *J. Low Temp. Phys.* **7**, 351 (1972).
3. P. W. Anderson, B. I. Halperin, C. M. Varma, *Philos. Mag.* **25**, 1 (1972).
4. W. A. Phillips, *Rep. Prog. Phys.* **50**, 1657 (1987).
5. W. A. Phillips, Ed., *Amorphous Solids: Low-Temperature Properties* (Springer, Berlin, Heidelberg, 1981).
6. C. Enss, S. Hunklinger, *Low-Temperature Physics* (Springer, Berlin, Heidelberg, 2005).
7. R. W. Simmonds *et al.*, *Phys. Rev. Lett.* **93**, 077003 (2004).
8. J. M. Martinis *et al.*, *Phys. Rev. Lett.* **95**, 210503 (2005).
9. J. Gao *et al.*, *Appl. Phys. Lett.* **92**, 212504 (2008).
10. S. Ashhab, J. R. Johansson, F. Nori, *New J. Phys.* **8**, 103 (2006).
11. G. Zolfagharkhani, A. Gaidarzhy, S. Shim, R. L. Badzey, P. Mohanty, *Phys. Rev. B* **72**, 224101 (2005).
12. F. Hoehne *et al.*, *Phys. Rev. B* **81**, 184112 (2010).
13. O. Arcizet, R. Riviere, A. Schliesser, G. Anetsberger, T. J. Kippenberg, *Phys. Rev. A* **80**, 021803 (2009).
14. A. Lupaşcu, P. Bertet, E. F. C. Driessen, C. J. P. M. Harmans, J. E. Mooij, *Phys. Rev. B* **80**, 172506 (2009).
15. J. Lisenfeld *et al.*, *Phys. Rev. B* **81**, 100511(R) (2010).
16. T. A. Palomaki *et al.*, *Phys. Rev. B* **81**, 144503 (2010).
17. M. Neeley *et al.*, *Nat. Phys.* **4**, 523 (2008).
18. J. Lisenfeld *et al.*, *Phys. Rev. Lett.* **105**, 230504 (2010).
19. A. M. Zagoskin, S. Ashhab, J. R. Johansson, F. Nori, *Phys. Rev. Lett.* **97**, 077001 (2006).
20. G. Sun *et al.*, *Nat. Commun.* **1**, 51 (2010).
21. G. J. Grabovskij *et al.*, *New J. Phys.* **13**, 063015 (2011).
22. W. A. Phillips, Ed., in *Amorphous Solids: Low-Temperature Properties* (Springer, Berlin, Heidelberg, 1981), pp. 53–64.
23. Supplementary materials are available on *Science* Online.
24. J. M. Martinis, *Quantum Inf. Process.* **8**, 81 (2009).
25. L. Faoro, J. Bergli, B. L. Altshuler, Y. M. Galperin, *Phys. Rev. Lett.* **95**, 046805 (2005).
26. L. Faoro, L. B. Ioffe, *Phys. Rev. B* **75**, 132505 (2007).
27. R. de Sousa, K. B. Whaley, T. Hecht, J. von Delft, F. K. Wilhelm, *Phys. Rev. B* **80**, 094515 (2009).
28. J. H. Cole *et al.*, *Appl. Phys. Lett.* **97**, 252501 (2010).
29. J. S. Kline, H. Wang, S. Oh, J. M. Martinis, D. P. Pappas, *Supercond. Sci. Tech.* **22**, 015004 (2009).
30. N. O. Birge, J. S. Moon, D. Hoadley, *Czech. J. Phys.* **46**, 2343 (1996).
31. S. Brouër, G. Weiss, H. B. Weber, *Europhys. Lett.* **54**, 654 (2001).

Acknowledgments: We thank M. Ansmann and J. M. Martinis (University of California, Santa Barbara) for providing the sample we measured in this work and J. H. Cole, E. Demler, Y. M. Galperin, M. D. Lukin, J. M. Martinis, R. McDermott, J. E. Mooij, C. Müller, A. Shnirman, and J. Wrachtrup for fruitful discussions. This work was supported by the DFG and the State of Baden-Württemberg through the DFG CFN, as well as by the European Union project SOLID.

Supplementary Materials

www.sciencemag.org/cgi/content/full/338/6104/232/DC1
Supplementary Text
Figs. S1 to S4
References (*32*–*35*)

25 June 2012; accepted 6 September 2012
10.1126/science.1226487

Observation of Resonances in Penning Ionization Reactions at Sub-Kelvin Temperatures in Merged Beams

A. B. Henson, S. Gersten, Y. Shagam, J. Narevicius, E. Narevicius*

Experiments have lagged theory in exploring chemical interactions at temperatures so low that translational degrees of freedom can no longer be treated classically. The difficulty has been to realize in the laboratory low-enough collisional velocities between neutral reactants to access this regime. We report here the realization of merged neutral supersonic beams and the manifestation of clear nonclassical effects in the resulting reactions. We observed orbiting resonances in the Penning ionization reaction of argon and molecular hydrogen with metastable helium, leading to a sharp absolute ionization rate increase in the energy range corresponding to a few degrees kelvin down to 10 millikelvin. Our method should be widely applicable to many canonical chemical reactions.

Theoretical quantum chemistry suggests that at low-enough collision energies, where reactants' de Broglie wavelength approaches the characteristic interaction length scale, quantum effects, such as tunneling through reaction or centrifugal barriers, will dominate the reaction

dynamics (*1*). So far, studies in this regime have largely been confined to theory because of the experimental challenge of achieving millikelvin collision energies. Among the reported observations of reactions at temperatures of 1 K or below (*2*–*5*), Ospelkaus *et al*. (*4*) presented evidence of nonclassical effects in the reaction of ultracold KRb molecules. In a different approach, Schreiner *et al*. (*6*) demonstrated that tunneling dominated isomerization reaction rates for molecules trapped in an argon matrix at 11 K. One of the most notable manifestations of quantum tunneling is the formation of scattering resonance states that can dramatically affect the reaction rate. Quasi-bound resonance states arise in the continuum portion of the spectrum, making them accessible to scattering experiments wherein the collision energy can be tuned. Detection of scattering resonances in reactions allows an accurate determination of the interaction potentials governing the collision dynamics. Such measurements constrain various theoretical models and methods, such as electronic structure calculations (that because of complexity always involve approximations) and molecular dynamics simulations that necessarily require quantum treatment at these low temperatures. Although dynamical Feshbach resonances have been measured in the differential cross-section of the $F + H_2$ reaction (*7*), so far tunneling resonances have not been observed in low-temperature reactive scattering.

We report here the observation of scattering resonances in the Penning ionization (PI) of argon and molecular hydrogen upon collisions with metastable helium atoms. PI is a fundamental reaction in nature between two neutral species leading to ionization by impact with an internally excited atom or molecule (*8*). This process is central to plasma chemistry (*9*) and has many applications, including surface characterization studies (*10*) and mass spectroscopy (*11*). PI falls into a large class of processes in physics that involve a discrete electronic state embedded into a continuum of states to which it is coupled, resulting in an autoionization process (*12*). However, the autoionizing collisional complex is only formed during a collision, and nuclear dynamics play a major role in PI reactions. We show that quantum effects in the nuclear motion strongly affect the ionization rate by observing sharp peaks arising from the formation of metastable collision complexes via quantum tunneling through an angular momentum barrier. Such a behavior is governed by the long-range interactions between the colliding species, is general to neutral-neutral collisions in the low-energy range, and has been predicted to occur in many reactive systems, including chemical (*13*–*17*) as well as PI reactions (*18*). The experimental breakthrough that enabled our observations was a merged beam approach that tuned collision temperatures down to 10 mK, despite the use of conventional supersonic molecular and atomic beams without any additional cooling stage. At 10-mK collision temperature, the corresponding de Broglie wavelength in the case of molecular hydrogen PI is 27 nm. The temperatures that we achieve are more than three orders of magnitude lower than those attainable in state-of-the-art systems featuring collision energy tunability. The advantage of reducing relative velocity, or collision energy, by merging two beams was recently theoretically investigated by Wei *et al*. (*19*), and we realized this idea by bending the trajectories in one of the beams with use of a curved magnetic quadrupole guide.

The history of angular momentum barrier tunneling, also called orbiting resonances, dates far back to the origins of collision theory. Boltzmann postulated that a collisional metastable complex forms during recombination reactions via an interaction with a third body (*20*). This possibility was later ruled out as improbable. Bunker recognized that the metastable intermediate state, formed by the colliding atoms and molecules, can be trapped by the potential barrier, which emerges from the contribution of the centrifugal potential (*21*). In the case of elastic scattering, the effect of the orbiting resonances on the elastic collision cross-section has been experimentally measured by making a very clever choice of collision partners, leading to a system with a low reduced mass and a weak van der Waals interaction strength (*22*–*24*). At these favorable conditions, orbiting resonances are formed at high collision energies equivalent to about 10 K. Shape resonances have been detected in the elastic scattering of laser-cooled atoms as well (*25*, *26*). Recently, Chefdeville *et al*. (*27*) observed resonance structure in inelastic scattering of CO molecules with molecular hydrogen above the excitation threshold temperature of 5 K.

Although the appearance of resonances in low-energy collisions is a rule rather than an exception, observations are confounded by the lowest collision energies available in experiments, as well as the requirement for a resolution high enough to discern individual resonance states. Practically, it is necessary to scan rates in an energy range corresponding to temperatures from a few degrees kelvin to a few millikelvin. Below several mK, only the *s*-wave scattering channel remains open, and the Wigner threshold law (*28*) reestablishes monotonic rate behavior.

Among the many available methods that permit tuning of the collision energy, none have reached temperatures sufficiently low to enable routine observation of resonances in the cold regime. Two ways to induce cold collisions are to perform the experiment in a cryogenic cell (*29*, *30*) or within a uniform supersonic expansion with carefully controlled temperature and density (*31*, *32*). Another school of thought, motivated by the pioneering experiments conducted by D. Herschbach and Y. T. Lee (*33*) involving the use of two crossed supersonic beams, aims to control the collision energy by varying the angle of collision or the velocity of one of the beams. Recently, adjustment of the crossing angle has been used to measure a reaction cross-section down to a temperature of 5 K (*34*). Meijer and colleagues used pulsed electric field decelerated supersonic beams to study inelastic scattering (*35*). Inelastic scattering experiments were also performed with magnetically trapped atoms and molecules (*36*, *37*) with the lowest temperature reported at 5 K (*38*).

In our approach, we were able to break through the 1-K collision temperature threshold by merging two fast supersonic beams: Relative velocity vanishes in a moving frame of reference when beams of equal velocities merge. Similar methods have been used in ion chemistry for almost two decades (*39*). In contrast to charged particles where trajectories can be easily controlled via interaction with modest electric fields, the neutral particles' center of mass motion is far more challenging to control. We used the Zeeman effect in order to direct paramagnetic species through a curved magnetic quadrupole guide. At the exit of the quadrupole, the paramagnetic particle beam merges with another supersonic beam that has travelled in a straight line from a separate supersonic source. There is no restriction on the nature

Department of Chemical Physics, Weizmann Institute of Science, Rehovot, Israel.

*To whom correspondence should be addressed. E-mail: edn@weizmann.ac.il

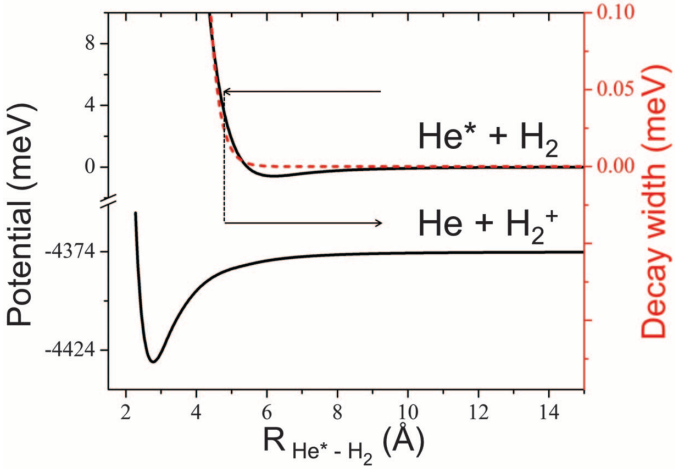

Fig. 1. The spherical portion of the interaction potentials involved in the PI reaction of metastable He (^{3}S) and molecular hydrogen. The entrance channel includes both the real part of the potential (top solid black line) as well as autoionization width (dashed red line). The bottom black curve represents the ion-neutral exit-channel interaction potential.

of the second beam, and any atom or molecule that can be entrained into the supersonic beam could be used in principle. By varying the relative velocities between the two beams, we continuously tune collisional energies from 350 K down to 10 mK. The lower bound for collision energy is unexpected. One would naïvely expect the lowest collision temperature we can achieve to be limited by the temperature of the hottest beam among the two, in the range of 0.1 to 1 K. The reduction in energy occurs because of longitudinal momentum compression in phase space during free propagation. Our nozzle-opening duration is much shorter compared with the propagation to the detector time, and the initial spherical phase space distribution deforms assuming a cigar shape.

In our study of low-energy PI reactions, we merged a supersonic beam of metastable helium with a supersonic beam containing either argon or molecular hydrogen. The excited ^{3}S state of helium has an energy of 19.8 eV above the ground state. When a metastable helium atom collides with another atom or molecule with an ionization energy lower than 19.8 eV, a charge-transfer process takes place whereby an electron from the neutral species jumps into the vacancy of the 1s orbital of helium, coinciding with the ejection of an electron from the 2s orbital to the continuum (Eq. 1)

$$He^* + M \rightarrow He + M^+ + e^- \qquad (1)$$

PI has been studied in detail at higher energies, with many interesting results summarized in a review article by Siska (*40*). PI reactions have different entrance and exit channels (Fig. 1). In the entrance channel, the interaction between metastable helium and another atom or molecule can be described by using a complex optical potential. The real part of the interatomic potential contains the appropriate long-range van der Waals interaction, the leading term of which scales as R^{-6}, where R is the distance between the metastable He atom and the colliding atom or molecule. At short distances the repulsion term takes over, whereas at intermediate distances there is a shallow van der Waals well. The complex part of the potential $\Gamma(R)/2$ is related to the ionization probability at a given internuclear distance. Because the charge transfer probability decays rapidly with separation, it is usually modeled by a single exponential term. Electronic motion is much faster compared with nuclear motion, and the autoionization process can be viewed as a vertical process within the Born Oppenheimer approximation. The resulting ion and neutral helium interaction is described by a neutral-ion potential surface in the exit channel.

A schematic of the experimental system is shown in Fig. 2A. The pulsed metastable helium supersonic beam was created by using an Even-Lavie valve (*41*) cooled down to 55 K. Immediately after the valve there is a dielectric barrier discharge (*42*), which was used to excite the ground-state helium to the 2^3S level. The beam had a mean velocity of ~770 m/s with a standard deviation of 15 m/s, corresponding to a temperature of 50 mK in the moving frame of reference. The beam then passed through a 4-mm-diameter skimmer located 10 cm from our valve orifice and entered a 20-cm-long magnetic quadrupole, which had a 10° curve with a curvature radius of 114.7 cm. We created a quadrupole magnetic field by passing a current pulse through 1-mm diameter copper wires arranged in quadratures, as shown in Fig. 2B; each quadrature consisted of nine wires in a three-by-three pattern. At the peak current of 1000 A, the transverse quadrupole trap depth was about 2.7 K and 3 mm by 3 mm in size. Only low-field–seeking Zeeman sublevels were confined in two dimensions during the transit through the quadrupole guide. As such, the metastable helium beam leaving the magnetic quadrupole was 100% spin-polarized in a single quantum state with the projection of the total

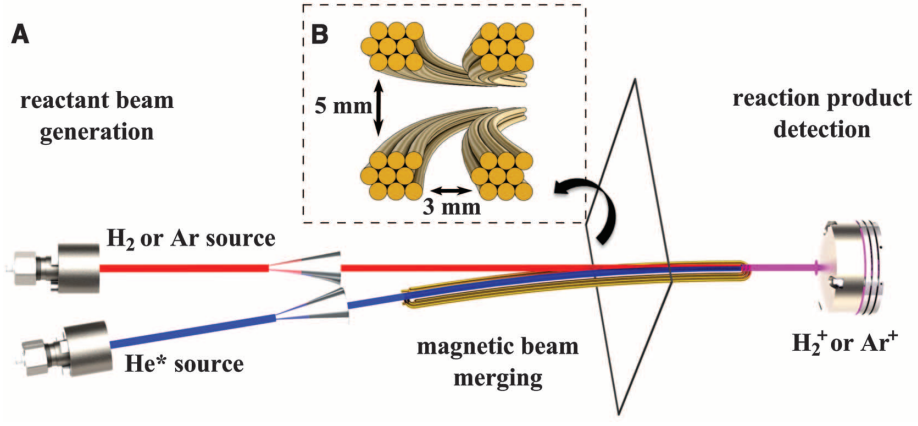

Fig. 2. (**A**) Schematic of the experimental system within the vacuum chambers, showing the two source supersonic valves followed by two skimmers, the curved magnetic quadrupole guide with its assembly, and the QMS entrance at the end. The blue beam is magnetically guided, whereas the red beam is unaffected. The merged volume is in purple. (**B**) A front view of the quadrupole guide.

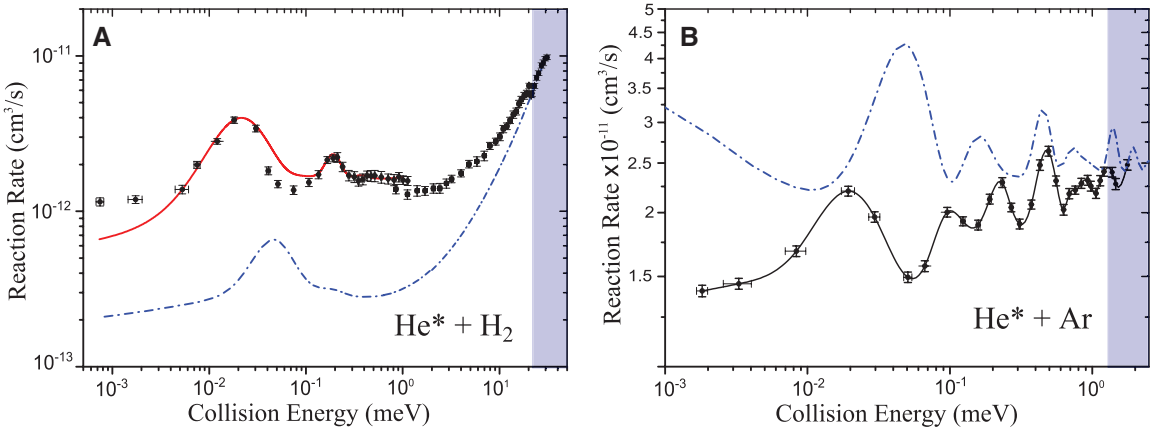

Fig. 3. (**A**) Reaction rate measurements for (^{3}S) He* and H_2 PI are shown in black with error bars. The lowest collision energy achieved is 0.75 with standard deviation of 0.07 μeV, corresponding to 8.7 ± 0.8 mK temperature. Blue dash-dot line is the reaction rate calculated by using the most recent potential from (*44*). Red solid line is the calculated reaction rate by using the Tang-Toennies potential with parameters that give the best fit to our measured results. A second slower decay term is included in the imaginary part of the potential in order to adjust the reaction rate value at low collision energies. (**B**) Reaction rate measurements for (^{3}S) He* and Ar PI are shown in black with error bars, and the solid black line is a guide to the eye. The blue dash-dot line is the reaction rate calculated by using the most recent experimental potential from (*43*). Shaded areas in both figures correspond to the energy range where our results overlap with the earlier measurements. The data points in (A) and (B) represent the mean ± standard deviations, where the reaction rate was determined by 50 measurements and the collision energy by 40 measurements.

angular momentum on the quantization axis, $m_J = 1$, originating from the ^3S electronic state manifold. At the end of the quadrupole, the metastable beam merged with a second supersonic beam, also created with a temperature-controlled Even-Lavie valve, and collimated with a 4-mm skimmer. This second beam contained molecular hydrogen in one experiment and atomic argon in another, either as neat gases or seeded in a noble carrier gas. By changing the composition of the gas mixtures as well as the temperature of the valve (between 355 and 120 K), we changed the relative mean velocity between the beams from over 1000 m/s down to zero. At zero relative velocity between the beams, the residual collision energy stems from the finite velocity distribution of the supersonic beams within the collision volume.

We measured the time-of-flight signal for both reactant beams as well as the product. The metastable beam was measured by using a microchannel plate, whereas the ground state beam was measured by using an ionizing quadrupole mass spectrometer (QMS). To measure the product ion, we turned off the ionizing element of the QMS in order to observe the ions formed in the chemi-ionization collisions. We first divided the ion signal by the product of the area of both neutral beams and then normalized by using the data from earlier high-collision-energy experiments (*43*, *44*). Thus, we are able to present our results for hydrogen (Fig. 3A) and for argon (Fig. 3B) on the absolute reaction rate scale.

At higher collision energies, above 1 meV (11.5 K) and 20 meV (230 K) for the Ar and H_2 systems, respectively, our results are in very good agreement with earlier experimental measurements. A classical treatment of the collisional process is sufficient to explain the main results above this energy. The reaction rate falls at lower velocities because the inner classical turning-point position scales with energy. For lower energies, the classical turning point is positioned at larger internuclear separation where the ionization rate is lower. At about 5 and 1 meV in the cases of Ar and H_2 ionization, respectively, the reaction rate levels off because the decrease of the ionization rate is compensated by longer collision times.

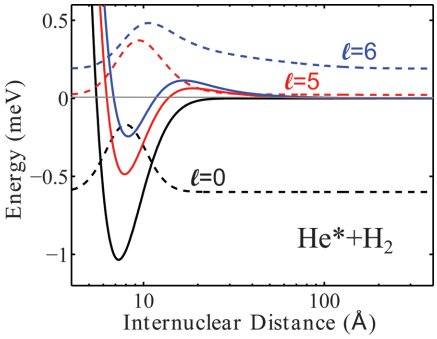

Fig. 4. Potentials and wave functions for the entrance channel of (^3S) He* and H_2 reaction. Potentials for different contributing angular momentum terms are shown as solid lines with the corresponding absolute values of wave functions as dashed lines. The black bottommost lines are for the potential with $l = 0$. Lines above that in red are for $l = 5$, and the topmost blue lines are for the $l = 6$ partial wave.

At energies below 1 meV, collisions enter the quantum regime, and we observed a series of peaks in the total reaction rate as a function of energy. Peaks appeared in the cases of PI of both argon and molecular hydrogen. The number of peaks and the peak spacing scales with the reduced mass, indicating that the quantization of the internuclear coordinate is involved. To elucidate the origins of the resonant structures, we have performed numerical simulations of the collision process. We numerically integrated the Schrödinger equation with a complex potential and for each partial wave determined the complex phase shift from the asymptotic behavior of the numerical solution. In case of H_2 PI, we used the spherical symmetric part of the potential similar to the treatment presented by Toennies (*24*). The total ionization reaction rate is given by a weighted sum over the contribution of individual partial waves.

We used the most recent potential energy surfaces (*44*) constructed by using both ab initio calculation results and experimental data obtained at higher energies. The potential correctly captures the higher energy behavior yet fails to reproduce the positions of the resonance states (Fig. 3A). Because the interaction potentials of metastable helium with molecular hydrogen have been thoroughly investigated by using ab initio methods, we chose this system to try to fit the potential surface parameters so as to match the observed resonance positions. We used a Tang-Toennies potential (*45*), starting with parameters derived from the most recent potential surface. We were able to match the resonance positions only after we increased the van der Waals potential well depth by a factor of 1.8 and moved the well minimum position by 1 Å. Such sensitivity to the parameters of the potential surface illustrates the importance of measuring the resonance states in order to obtain the correct long-range interaction behavior. Furthermore, these experiments should stimulate theoretical investigations of the metastable helium-molecular hydrogen potential resulting from the system's simplicity, because it involves only four electrons and thus can serve as a benchmark for different ab initio methods. In addition to the mismatch in the positions of the resonance peaks, there was also a discrepancy, at low energies, of almost an order of magnitude between the measured and calculated reaction rates. The observed higher reaction rate can be reproduced in our calculations by the addition of a slower decay term to the imaginary part of the potential. This raises the question of whether the estimation of an autoionization width as a single decaying exponent is sufficiently accurate. This discrepancy could possibly arise from the underestimation of atomic and molecular orbital overlap at large separations.

We have also calculated the resonance wave functions by using discrete variable representation (*46*) and complex scaling methods (*47*). In the case of molecular hydrogen PI, the resonant states appear in the partial waves associated with the total angular momentum $l = 5$ and 6 (Fig. 4). The orbiting resonance wave functions are highly delocalized, extending to more than 10 Å. The orbiting resonance associated with the $l = 6$ partial wave channel has an energy above the centrifugal barrier. Such a resonance is formed by a quantum reflection off, and not tunneling through, the angular momentum barrier.

The resonance wave functions illustrate the mechanism of low-energy resonant chemi-ionization. Classically, one would expect that collisions of particles at energies below the centrifugal barrier should not contribute to the ionization process. However, at collision energies that match positions of the resonance states, particles tunnel through the centrifugal barrier and become trapped. In such a case, the probability of finding colliding particles, described by the absolute value of corresponding wave function, is enhanced inside of the centrifugal barrier within the region where the autoionization rate is higher.

Our results manifest a quantum effect in ionization reactions below 1 K. We have observed orbiting resonances in the PI reaction of molecular hydrogen and argon with metastable helium that proceed by tunneling through an angular momentum potential barrier. As a result, we observed sharp peaks in the reaction rate measurements as a function of collision energy. The application of our method toward studying chemical reactions is straightforward. Atomic and molecular radical collisional partners are paramagnetic, and as such their beams can be manipulated by using our curved magnetic quadrupole. For example, a beam of atomic fluorine can be turned and merged with molecular hydrogen in order to study the canonical $F + H_2$ reaction in the cold regime where the reaction proceeds via tunneling. The theory of this chemical reaction suggests that resonances exist in the sub-kelvin energy range (*48*) and should be accessible by using our method.

References and Notes

1. R. V. Krems, *Phys. Chem. Chem. Phys.* **10**, 4079 (2008).
2. S. Willitsch, M. T. Bell, A. D. Gingell, S. R. Procter, T. P. Softley, *Phys. Rev. Lett.* **100**, 043203 (2008).
3. T. L. Mazely, M. A. Smith, *Chem. Phys. Lett.* **144**, 563 (1988).
4. S. Ospelkaus *et al.*, *Science* **327**, 853 (2010).
5. V. Singh *et al.*, *Phys. Rev. Lett.* **108**, 203201 (2012).
6. P. R. Schreiner *et al.*, *Science* **332**, 1300 (2011).
7. M. Qiu *et al.*, *Science* **311**, 1440 (2006).
8. M. J. Druyvesteyn, F. M. Penning, *Rev. Mod. Phys.* **12**, 87 (1940).
9. A. Fridman, *Plasma Chemistry* (Cambridge Univ. Press, Cambridge, 2008).
10. Y. Harada, S. Masuda, H. Ozaki, *Chem. Rev.* **97**, 1897 (1997).
11. R. B. Cody, J. A. Laramée, H. D. Durst, *Anal. Chem.* **77**, 2297 (2005).
12. W. H. Miller, *J. Chem. Phys.* **52**, 3563 (1970).

13. N. Balakrishnan, A. Dalgarno, *Chem. Phys. Lett.* **341**, 652 (2001).
14. E. Bodo, F. A. Gianturco, A. Dalgarno, *J. Chem. Phys.* **116**, 9222 (2002).
15. D. W. Chandler, *J. Chem. Phys.* **132**, 110901 (2010).
16. P. F. Weck, N. Balakrishnan, *J. Chem. Phys.* **122**, 154309 (2005).
17. G. Quéméner, N. Balakrishnan, B. K. Kendrick, *J. Chem. Phys.* **129**, 224309 (2008).
18. B. Brutschy, H. Haberland, K. Schmidt, *J. Phys. B* **9**, 2693 (1976).
19. Q. Wei, I. Lyuksyutov, D. Herschbach, *J. Chem. Phys.* **137**, 054202 (2012).
20. L. Boltzmann, *Vorlesung Uber Gastheorie II* (J. A. Barth, Leipzig, Germany, 1989).
21. D. L. Bunker, N. Davidson, *J. Am. Chem. Soc.* **80**, 5085 (1958).
22. A. Schutte, D. Bassi, F. Tommasini, G. Scoles, *Phys. Rev. Lett.* **29**, 979 (1972).
23. J. P. Toennies, W. Welz, G. Wolf, *J. Chem. Phys.* **61**, 2461 (1974).
24. J. P. Toennies, W. Welz, G. Wolf, *J. Chem. Phys.* **71**, 614 (1979).
25. Ch. Buggle, J. Léonard, W. von Klitzing, J. T. M. Walraven, *Phys. Rev. Lett.* **93**, 173202 (2004).
26. N. R. Thomas, N. Kjaergaard, P. S. Julienne, A. C. Wilson, *Phys. Rev. Lett.* **93**, 173201 (2004).
27. S. Chefdeville *et al.*, *Phys. Rev. Lett.* **109**, 023201 (2012).
28. E. P. Wigner, *Phys. Rev.* **73**, 1002 (1948).
29. J. M. Doyle, B. Friedrich, J. Kim, D. Patterson, *Phys. Rev. A* **52**, R2515 (1995).
30. C. D. Ball, F. C. De Lucia, *Phys. Rev. Lett.* **81**, 305 (1998).
31. B. R. Rowe, G. Dupeyrat, J. B. Marquette, P. Gaucherel, *J. Chem. Phys.* **80**, 4915 (1984).
32. I. W. M. Smith, *Angew. Chem. Int. Ed.* **45**, 2842 (2006).
33. Y. T. Lee, J. D. Mcdonald, P. R. Lebreton, D. Herschbach, *Rev. Sci. Instrum.* **40**, 1402 (1969).
34. C. Berteloite *et al.*, *Phys. Rev. Lett.* **105**, 203201 (2010).
35. J. J. Gilijamse, S. Hoekstra, S. Y. T. van de Meerakker, G. C. Groenenboom, G. Meijer, *Science* **313**, 1617 (2006).
36. L. P. Parazzoli, N. J. Fitch, P. S. Żuchowski, J. M. Hutson, H. J. Lewandowski, *Phys. Rev. Lett.* **106**, 193201 (2011).
37. B. C. Sawyer, B. K. Stuhl, D. Wang, M. Yeo, J. Ye, *Phys. Rev. Lett.* **101**, 203203 (2008).
38. B. C. Sawyer *et al.*, *Phys. Chem. Chem. Phys.* **13**, 19059 (2011).
39. R. H. Neynaber, in *Advances in Atomic and Molecular Physics*, D. R. Bates, E. Immanuel, Eds. (Academic Press, New York, 1969), vol. 5, pp. 57–108.
40. P. E. Siska, *Rev. Mod. Phys.* **65**, 337 (1993).
41. U. Even, J. Jortner, D. Noy, N. Lavie, C. Cossart-Magos, *J. Chem. Phys.* **112**, 8068 (2000).
42. K. Luria, N. Lavie, U. Even, *Rev. Sci. Instrum.* **80**, 104102 (2009).
43. S. Burdenski, R. Feltgen, F. Lichterfeld, H. Pauly, *Chem. Phys. Lett.* **78**, 296 (1981).
44. D. W. Martin, C. Weiser, R. F. Sperlein, D. L. Bernfeld, P. E. Siska, *J. Chem. Phys.* **90**, 1564 (1989).
45. K. T. Tang, J. P. Toennies, *J. Chem. Phys.* **80**, 3726 (1984).
46. D. T. Colbert, W. H. Miller, *J. Chem. Phys.* **96**, 1982 (1992).
47. N. Moiseyev, *Non-Hermitian Quantum Mechanics* (Cambridge Univ. Press, Cambridge, 2011).
48. F. Lique, G. Li, H. -J. Werner, M. H. Alexander, *J. Chem. Phys.* **134**, 231101 (2011).

Acknowledgments: We acknowledge U. Even for many helpful discussions and sound advice. We thank R. Ozeri for most fruitful discussions; M. Raizen, R. Naaman, Y. Prior, and B. Dayan for a careful reading of the manuscript; and S. Assayag and M. Vinetsky from the Weizmann machine shop for assistance in designing and manufacturing of our vacuum chamber. This research was made possible, in part, by the historic generosity of the Harold Perlman Family. E.N. acknowledges support from the Israel Science Foundation and Minerva Foundation.

2 July 2012; accepted 6 September 2012
10.1126/science.1229141

An Ancient Core Dynamo in Asteroid Vesta

Roger R. Fu,[1]* Benjamin P. Weiss,[1] David L. Shuster,[2,3] Jérôme Gattacceca,[4] Timothy L. Grove,[1] Clément Suavet,[1] Eduardo A. Lima,[1] Luyao Li,[1] Aaron T. Kuan[5]

The asteroid Vesta is the smallest known planetary body that has experienced large-scale igneous differentiation. However, it has been previously uncertain whether Vesta and similarly sized planetesimals formed advecting metallic cores and dynamo magnetic fields. Here we show that remanent magnetization in the eucrite meteorite Allan Hills A81001 formed during cooling on Vesta 3.69 billion years ago in a surface magnetic field of at least 2 microteslas. This field most likely originated from crustal remanence produced by an earlier dynamo, suggesting that Vesta formed an advecting liquid metallic core. Furthermore, the inferred present-day crustal fields can account for the lack of solar wind ion-generated space weathering effects on Vesta.

The terrestrial planets are thought to have formed from the successive growth and accretion of protoplanetary objects <1000 km in diameter (*1*). A fraction of these protoplanets have survived to the present day and include 4 Vesta, the second most massive asteroid (525 km mean diameter). In particular, Vesta's high density, primordial basaltic crust, and large size suggest that it is an intact remnant of the early solar system that escaped catastrophic collisional disruption (*2*). Vesta therefore provides an opportunity to characterize the building blocks of the terrestrial planets and to study the processes of planetesimal accretion and differentiation.

Meteorites of the howardite-eucrite-diogenite (HED) clan probably sample the crust and upper mantle of Vesta (*3*). Geochemical studies of HED meteorites suggest that Vesta has a fully differentiated structure, with a metallic core ranging from 5 to 25% of the total planetary mass (*4*) that formed within ~1 to 4 million years (My) of the beginning of the solar system (*5, 6*). Recent volume and mass constraints from the NASA Dawn mission provide evidence of a metallic core between 107 and 113 km in radius (*2*).

Vigorous advection in a molten metallic core may generate a dynamo magnetic field. Paleomagnetic studies of meteorites suggest that past dynamos may have existed on other asteroidal objects such as the angrite and the CV carbonaceous chondrite parent bodies (*7, 8*). These data offer the possibility of studying the physics of dynamo action in a small-body regime not represented by active dynamos in the solar system today, in which Mercury is the smallest body with a known active dynamo (*9*). However, there has been no meteorite group for which evidence of dynamo action has been confidently established and that has been directly associated with a known, intact, asteroidal parent body.

Previous paleomagnetic studies have shown that many HED meteorites are low-fidelity recorders of magnetic fields because of their large (i.e., multidomain), low-coercivity magnetic minerals (*10*). Furthermore, these paleomagnetic studies generally lacked radiometric ages and thermochronometry. As a result, they came to no firm conclusions about the origin of magnetization identified in HED meteorites (*11*). Although dynamo-generated and even nebular fields were considered, other potential sources such as recent magnetic contamination and impact-generated fields could not be ruled out (*10, 12–14*). Here, we present a paleomagnetic study of ALHA81001 (ALH, Allan Hills), a meteorite found in Antarctica in 1981 with exceptional magnetic recording properties (*15*). We also present thermochronologic and petrographic data that constrain the origin of the meteorite's natural remanent magnetization (NRM).

The main–HED-group oxygen isotopic composition of ALHA81001 suggests that it originated on Vesta (*16*). As a eucrite, ALHA81001 has a basaltic composition and probably is a sample of the asteroid's upper crust. Our petrographic observations show that ~99 volume % of ALHA81001 has a fine-grained texture. A previous paleomagnetic study found that ALHA81001 has one of the most stable NRM records observed for any main–oxygen-isotope group HED

[1]Department of Earth, Atmospheric, and Planetary Sciences, Massachusetts Institute of Technology, 77 Massachusetts Avenue, Cambridge, MA 02139, USA. [2]Department of Earth and Planetary Science, University of California, Berkeley, CA 94720, USA. [3]Berkeley Geochronology Center, 2455 Ridge Road, Berkeley, CA 94709, USA. [4]Centre Européen de Recherche et d'Enseignement des Géosciences de l'Environnement, CNRS/Université Aix-Marseille 3, France. [5]Department of Applied Physics, Harvard University, Cambridge, MA 02138, USA.

*To whom correspondence should be addressed. E-mail: rogerfu@mit.edu

Observation of Resonances in Penning Ionization Reactions at Sub-Kelvin Temperatures in Merged Beams

A. B. Henson, S. Gersten, Y. Shagam, J. Narevicius and E. Narevicius

Science **338** (6104), 234-238.
DOI: 10.1126/science.1229141

Relatively Cold

Temperature is essentially a measure of relative atomic or molecular motion. Low temperature does not necessarily imply a sample at absolute rest––what is important is for every member of the sample to be moving (or not moving) at the same velocity. Techniques for studying reactions under extreme cooling have nonetheless tended to focus on slowing down molecules. **Henson *et al.*** (p. 234) now demonstrate an alternative approach in which two beams of distinct gas-phase reagents are merged so as to continue forward with very little spread in their velocity. The interactions thus occur at millikelvin temperatures, revealing signatures of nonclassical dynamics such as oscillatory ionization probabilities with small shifts in energy.